



**HAL**  
open science

## When anthraquinone dyes meet pillared montmorillonite: Stability or fading upon exposure to light?

Pollyana Trigueiro, Francisco A.R. Pereira, David Guillermin, Baptiste Rigaud, Sébastien Balme, Jean-Marc Janot, Ieda M.G. dos Santos, Maria G. Fonseca, Philippe Walter, Maguy Jaber

### ► To cite this version:

Pollyana Trigueiro, Francisco A.R. Pereira, David Guillermin, Baptiste Rigaud, Sébastien Balme, et al.. When anthraquinone dyes meet pillared montmorillonite: Stability or fading upon exposure to light?. *Dyes and Pigments*, 2018, 159, pp.384-394. 10.1016/j.dyepig.2018.06.046 . hal-01871692

**HAL Id: hal-01871692**

<https://hal.umontpellier.fr/hal-01871692v1>

Submitted on 18 Jan 2019

**HAL** is a multi-disciplinary open access archive for the deposit and dissemination of scientific research documents, whether they are published or not. The documents may come from teaching and research institutions in France or abroad, or from public or private research centers.

L'archive ouverte pluridisciplinaire **HAL**, est destinée au dépôt et à la diffusion de documents scientifiques de niveau recherche, publiés ou non, émanant des établissements d'enseignement et de recherche français ou étrangers, des laboratoires publics ou privés.

1 When anthraquinone dyes meet pillared montmorillonite:  
2 stability or fading upon exposure to light?

3

4 Pollyana Trigueiro<sup>1,2</sup>, Francisco Rodrigues Pereira<sup>1,3</sup>, David Guillemin<sup>1</sup>, Baptiste Rigaud<sup>4</sup>, Sebastien  
5 Balme<sup>5</sup>, Jean-Marc Janot<sup>5</sup>, Ieda M. G. dos Santos<sup>6</sup>, Maria G. Fonseca<sup>6</sup>, Philippe Walter<sup>1</sup>, Maguy  
6 Jaber<sup>1\*</sup>

7

8 <sup>1</sup>Universités, UPMC Paris06, UMR 8220, Laboratoire d'Archéologie Moléculaire et Structurale, 4 place  
9 Jussieu, F-75005 Paris, France

10 <sup>2</sup>Materials Engineering Department of Universidade Federal da Paraíba, João Pessoa, Paraíba, Brazil

11 <sup>3</sup>Chemistry Department of Universidade Estadual da Paraíba, Campina Grande, Paraíba, Brazil

12 <sup>4</sup>CNRS Institut des Matériaux de Paris Centre (FR2482), 4 place jussieu, 75005 Paris, France

13 <sup>5</sup>Institut Européen des Membranes, UMR 5635, Université de Montpellier, ENSCM, CNRS, Place Eugène  
14 Bataillon, F-34095 Montpellier cedex 5, France

15 <sup>6</sup>Chemistry Department of Universidade Federal da Paraíba, João Pessoa, Paraíba, Brazil

16 <sup>7</sup>Materials Engineering Department of Universidade Federal do Piauí, Teresina, Piauí, Brazil

17

18

19 Corresponding authors

20 \*Maguy Jaber : [maguy.jaber@upmc.fr](mailto:maguy.jaber@upmc.fr)

21

22

23

24

25 **Abstract**

26 Hybrid pigments have attracted great interest due to their stability and physicochemical  
27 properties that can be used in paintings, artworks and in the field of cultural heritage. The  
28 study of new materials includes the search for new pigments by immobilization of the dyes in  
29 resistant substrates such as clays and minerals to get new colorants and materials with high  
30 stability. Organic-inorganic based lake pigments, at different pH, have been prepared. Ti- and  
31 Al-pillared montmorillonite were synthesized and loaded with carminic acid (CA) and alizarin  
32 (Aliz) organic dyes. The pillaring process was investigated by X-ray diffraction, textural  
33 analysis, transmission electron microscopy and solid state nuclear magnetic resonance of  
34  $^{27}\text{Al}$ . The interactions between the organic guest and the inorganic host were highlighted by  
35 infrared,  $^{13}\text{C}$  and  $^{27}\text{Al}$  solid state magnetic nuclear resonance and time resolved fluorescence  
36 spectroscopies. The spectra support complex formation between the chromophores and the  
37 inorganic matrix. The colours of the pigments prepared were pH dependent. Lake pigments  
38 based on Al-Pillared Mt were more stable under light than Ti-based hybrid, even in oil  
39 painting formulations.

40 Keywords: Hybrid pigment, Pillared clay, Carminic acid, Alizarin, NMR, Fluorescence,  
41 Photoaging.

42

43

44

## 45 **1.0 Introduction**

46

47 Through centuries, paintings have represented the expression through art of some  
48 characteristics of human and social behaviour, also reflecting the impacts of environmental  
49 aspects. However, the poor stability of the colours used against acids, light or temperature has  
50 been a serious problem that has affected works of art and aspects of their cultural heritage as  
51 result of their public exposure. Thus, designs for stable pigments are desired in order to  
52 prepare/restore paintings and overcome the problem of degradation [1]. It has been expected  
53 that the surface where pigments are applied is a preponderant factor in determining the  
54 efficiency/stability of colours, and the perfection of paintings. Although there are many  
55 sources, there is a necessity to find combinations of raw materials for use as colouring  
56 agents/colourants in ink formulations. In fact, hybrid pigments have wide applications not  
57 only in works of art, but also in the fields of optics, food processing, cosmetics or plastics [2–  
58 4]. Hybrid based on organic dye-inorganic compounds are chemically obtained by a strong  
59 interaction between organic chromophores and inorganic matrices aiming to obtain stable  
60 pigments [8] or removing anionic dyes from wastewater [5]. In this context, a growing  
61 application of inorganic dyes-based hybrids are established [6–8].

62 Anthraquinones are classified as the natural organic dyes most resistant to light-induced  
63 deterioration used since prehistoric times [9]. These red colourants may be extracted from the  
64 roots of a diversity of plants from the Rubiaceae family (madder family). Alizarin and  
65 purpurin are the principal occurring dyes in *Rubia tinctoria L.* (madder genus) [2,9]. Lakes are  
66 pigments formed from a dye-inorganic hybrid. Several other guest dyes have been reported in  
67 the literature to obtain lake pigments, such as carminic acid [1,8], fluorescein [8], betalain  
68 [10] and eosin [11].

69 Clays have attracted broad attention in the field of lake pigments because they are  
70 environment-friendly and low-cost materials and abundant in nature. Furthermore, some clay  
71 properties, such as high adsorption capacity and great potential for ion exchange, highlight  
72 their use as an inorganic support [12,13]. There are many confirmed examples of their use in  
73 clay-based lake pigments throughout history. A well-known example is “Maya Blue” which is  
74 a combination of indigo derived from the leaves of the local *añil* plant (*Indigofera*  
75 *suffruticosa*) with palygorskite, a clay mineral of fibrous nature found in the Yucatán  
76 Peninsula [14]. The hybrid compound has conserved a strong blue colour in Mayan artworks  
77 up to this day. Recently, it has been some papers have reported clay-based lake pigments such  
78 as Maya Blue-like [15], acid-activated sepiolite/Rhodamine B@SiO<sub>2</sub> fluorescent pigments  
79 [16], Halloysite/CoAl<sub>2</sub>O<sub>4</sub> hybrid pigments [7], Attapulgite/Fe (III) hybrid red pigments [3],  
80 Fe<sub>2</sub>O<sub>3</sub> supported on sepiolite or halloysite [17], Carminic acid onto montmorillonite [1].  
81 Among clay minerals, montmorillonite has attracted remarkable attention in the field of lake-  
82 based hybrids due to its peculiar features, such as swelling with a larger lamellar expansion  
83 capacity in aqueous solution. Moreover, its surface area negatively charged in an acid  
84 medium, enables it to interact with bulky molecules, such as cationic dyes [1,18].  
85 Montmorillonite is a 2:1 type clay mineral, member of smectite group, with a hydrous layered  
86 aluminium silicate with a high cationic exchange capability (CEC) and active hydroxyl  
87 groups [19]. Its layers consist of two tetrahedral silica sheets sandwiching one octahedral  
88 aluminium sheet. The cationic layered clays can be transformed into highly porous structures  
89 by a process known as pillarization. Pillaring provides chemical and thermal stability to clays  
90 as well as increasing interlayer space and surface area [20,21]. The most common type of  
91 pillared clays is obtained by the incorporation of aluminium polyhydroxylations in the  
92 interlayer space of the clay, calcination is essential to ensure the formation of nanoscale

93 alumina particles in the material [20,21]. Additionally, many other polycations formed upon  
94 hydrolysis of  $Zr^{4+}$ ,  $Ti^{4+}$ ,  $Cr^{3+}$ ,  $Fe^{3+}$  or  $Ga^{3+}$  were reported for pillaring clays [21,22].

95 In this perspective, the present investigation aimed to synthesize Ti- and Al-pillared  
96 montmorillonite and evaluate their influences on the photostability of new lake pigments and  
97 oil painting formulations. Alizarin (1,2-dihydroxyanthraquinone) and carminic acid (7-C- $\alpha$ -  
98 glucopyranosyl-3,5,6,8-tetrahydroxy-1-methyl-2-anthraquinone carboxylic acid) were used as  
99 dyeing agents.

100

## 101 **2.0 EXPERIMENTAL**

102 All chemicals applied in this work were purchased from Aldrich or Sigma-Aldrich with an  
103 analytical grade and used without any previous purification.

### 104 *2.1 Montmorillonite (Mt) synthesis*

105 The reagents were mixed in the following order: deionized water, hydrofluoric acid and the  
106 sources of interlamellar cation sodium acetate, magnesium acetate, alumina and silica. The  
107 hydrogel with the molar composition of  $SiO_2 \cdot 0.2Al_2O_3 \cdot 0.4MgO \cdot 0.05Na_2O \cdot xH_2O$  was aged  
108 under stirring at room temperature for 2 h and then was autoclaved at 220 °C for 72 h [19,23].

109 The autoclaves were cooled to room temperature and the product were washed thoroughly  
110 with distilled water and centrifuged. Finally, the obtained Mt was dried at 50 °C for 72 h.

### 111 *2.2 Pillaring process of Montmorillonite (PILC)*

112 The procedures for the pillaring process of Mt with aluminium polyhydroxycations and  
113 titanium ions followed the procedures adapted from Bergaoui et al [24] and Tomul et al [25],  
114 respectively.

115 For aluminium, the pillaring solution was obtained by hydrolysis of aluminium chloride with  
116 a NaOH solution up to OH:Al ratio of 2.2 and final concentration of 0.1 mol.L<sup>-1</sup>. This mixture  
117 was left to stand for 24 h at room temperature under stirring. Meanwhile, 3.2 g.L<sup>-1</sup> of the  
118 aqueous clay suspension (7.3 mmol Al<sup>3+</sup>.g clay) was aged under stirring at room temperature  
119 for 3 h. Then, aluminium solution was added dropwise to a clay suspension with flow of 1  
120 mL.min<sup>-1</sup>. The resulting solution was stirred 24 h at room temperature, washed and dried at 50  
121 °C for 24 h. The samples upon aluminium cations intercalation were denoted Al-Mt. The  
122 samples were calcined up to 500 °C for 2 h. The pillared clay samples with aluminium cations  
123 were denoted PILC-Al.

124 For titanium, the pillaring solution was prepared by hydrolysis of titanium isopropoxide with  
125 6 M HCl solution with Ti<sup>4+</sup>:H<sup>+</sup> molar ratio at 1:4. Titanium source solution was added  
126 dropwise with flow of 0.4 mL.min<sup>-1</sup> and the result solution was left stirring at room  
127 temperature for 6 h. Then, deionized water was added until reaching a concentration of 1 M  
128 H<sup>+</sup> and 0.25 M Ti<sup>4+</sup>. The pillaring solution was introduced dropwise with a flow of 1 mL.min<sup>-1</sup>  
129 to the Mt suspension until to reach 10 mmol Ti<sup>4+</sup>.g clay. The resulting suspension was stirred  
130 for 24 h at room temperature and then washed with deionized water until total chloride  
131 removal. The prepared solid was recovered by centrifugation and dried at 50 °C for 24 h.  
132 Samples upon titanium cations intercalation were denoted Ti-Mt. The samples were calcined  
133 up to 400 °C for 2 h. Pillared clay samples with titanium cations were denominated as PILC-  
134 Ti.

### 135 *2.3 Dyeing procedure*

136 Pillared montmorillonite was loaded with alizarin (Aliz) and carminic acid (CA) considering  
137 the different values of pK<sub>a</sub>. It is known that carminic acid presents three different values of

138 pK<sub>a</sub> (2.8, 5.4 and 8.1) [1,26], while alizarin has only two values (6.6 - 7.5 and 12.4 - 13.5)  
139 [9,27].

140 For each sample, 300 mg of pillared montmorillonite was added to 100 mL of carminic acid  
141 (0.6 g.L<sup>-1</sup>) or alizarin (0.8 g.L<sup>-1</sup>) solution and was left under stirring for 4 h. The samples were  
142 then centrifugated, washed with deionized water and dried at 50 °C for 24 h.

#### 143 *2.4 Oil painting formulation*

144 All the formulations were obtained by incorporating 35 mg of pigment in 400 µL of linseed  
145 oil. The mixture was then grinded and an homogeneous paste is obtained. Films were then  
146 prepared on slice glasses using specific applicator. Linseed oil is one of the earliest and the  
147 most commonly vehicle applied to ink formulations that remains been used nowadays.

### 148 **3.0 CHARACTERIZATIONS**

#### 149 *3.1 X-ray diffraction (XRD)*

150 Powder X-ray diffractograms were recorded using D8 Advance Bruker-AXS Powder X-ray  
151 diffractometer with CuK<sub>α</sub> radiation ( $\lambda = 1.5405 \text{ \AA}$ ). XRD patterns were performed between 5-  
152 70° (2 $\theta$ ) with scan rate of 0.5 deg.min<sup>-1</sup>. The active area of the detector was limited as much  
153 as possible in order to reduce the background scattering at low angle between 2-10° (2 $\theta$ ).

#### 154 *3.2 Textural investigation*

155 Nitrogen adsorption-desorption isotherms were measured at liquid nitrogen temperature on a  
156 Micromeritics ASAP 2020 apparatus. The specific surface area (S<sub>BET</sub>) was evaluated using the  
157 Brunauer-Emmett-Teller (BET) method. The pore size distribution was determined from the  
158 desorption part of the isotherm using the Barret-Joyner-Halender (BJH) method [28].

#### 159 *3.3 Transmission electron microscopy (TEM)*

160 TEM study of the samples was performed on a JEOL 2010 microscope, 200 kV LaB<sub>6</sub> coupled  
161 Orius camera, from Gatan Company. Samples in the form of bulk powders were suspended in  
162 ethanol and then deposited on 400 mesh copper grids covered with an ultrathin carbon  
163 membrane of 2 – 3 nm thickness.

#### 164 *3.4 ATR-FTIR*

165 Infrared analyzes was performed on Agilent Cary 630 FTIR spectrometer using Agilent  
166 diamond Attenuated Total Reflectance (ATR) technique mode, being spectral resolution > 2  
167 cm<sup>-1</sup> and 32 scans. Spectra were acquired by Microlab FTIR Software (Agilent Technologies).  
168 Spectra were acquired between 4000 and 650 cm<sup>-1</sup>.

#### 169 *3.5 Thermal Analysis (TG/DTG)*

170 Thermogravimetric analyses were carried out using a TA Instrument SDT Q600 analyzer. The  
171 heating rate was of 5 °C.min from 25 °C to 800 °C, under dry air flow of 10 mL.min, and  
172 using alumina pan.

#### 173 *3.6 Solid state nuclear magnetic resonance (<sup>13</sup>C CP-MAS and <sup>27</sup>Al MAS-NMR)*

174 <sup>13</sup>C and <sup>27</sup>Al MAS NMR spectra were obtained on a Bruker Avance III spectrometer equipped  
175 with a 4 mm H-X MAS probe, operating at frequency of 500.17 MHz (<sup>1</sup>H), 125.77 MHz (<sup>13</sup>C)  
176 and 130.33 MHz (<sup>27</sup>Al). Chemical shifts were calibrated using the carboxyl signal of  
177 adamantane (38.52 ppm) for <sup>13</sup>C and AlNO<sub>3</sub> (0 ppm) for <sup>27</sup>Al as external standard.

178 The <sup>13</sup>C Cross-Polarization spectra were acquired with a MAS rate of 14 kHz, a ramp-CP  
179 contact time of 1 ms and a 1 s recycle delay and with a <sup>1</sup>H decoupling spin. Over an  
180 acquisition time of 40 ms, the number of scans to obtain the spectra depends on the S/N  
181 obtained for each sample. Spectra were processed with a zero-filling factor of 2 and with an

182 exponential decay corresponding to a 25 Hz line broadening in the transformed spectra. Only  
183 spectra with the same line broadening are directly compared.

184 The  $^{27}\text{Al}$  experiment using  $30^\circ$  pulse is recorded in the same condition of spinning rate, 100  
185 kHz spectral width and with 500 ms recycle delay.

### 186 *3.7 Fluorescence Characterisation*

187 Time-resolved fluorescence spectroscopy was obtained by the time-correlated single-photon  
188 counting technique on lab-made device previously described [23,29]. For the analysis the  
189 fluorescence decay law at the magic angle  $I_M(t)$  were analyzed as a sum of exponentials:

$$190 \quad I_M(t) = \frac{1}{3} \sum_{i=1}^n \alpha_i e^{-t/\tau_i} \quad (\text{eq 1})$$

191 Where,  $\tau_i$  is the fluorescence lifetime and  $\alpha_i$  is the pre-exponential factor related to the  
192 contribution of each lifetime of the component  $i$ .

193 Fluorescence lifetimes were calculated from data collected at magic angle by iterative  
194 adjustment after convolution of a pump profile (scattered light) with a sum of exponentials as  
195 described previously. The criteria to evaluate the quality of fit are  $\chi^2$  the and the residue  
196 function. The fluorescent decay was recorded at  $\lambda_{\text{em}}=600$  nm under excitation  $\lambda_{\text{ex}}=540$  nm or  
197  $\lambda_{\text{em}}=550$  nm for carminic acid and alizarin, respectively.

### 198 *3.8 Light-Induced Aging*

199 Aging effects were simulated by exposure of solid pigments and oil paint formulations to  
200 white light irradiation for 340 hours, using a LED lamp set to provide 50 Klx of illumination  
201 intensity.

202 Spectrophotocolorimetry was performed using an Ocean Optics Halogen and Deuterium Light  
203 Source HL-2000-FHSA device as incident light beam and ocean optics USB4000 detector for

204 acquisition. Ocean Optics QP400-1-UV-VIS fiberglass was used to link these devices. For  
205 each acquisition, an average of 100 scans were useful to obtain the optimum signal. The  
206 reflectance wavelength range was set from 400 to 950 nm and measurements are done on  
207 pressed pellets samples as function of  $L^*$ ,  $a^*$  and  $b^*$  coordinates. The differences of colours  
208 between unexposed and exposed samples were calculated by  $\sqrt{((\Delta L^*)^2 + (\Delta a^*)^2 +$   
209  $(\Delta b^*)^2)}$  equation, according to the “Commission Internationale of l’Eclairage” (CIE).

## 210 4.0 RESULTS AND DISCUSSIONS

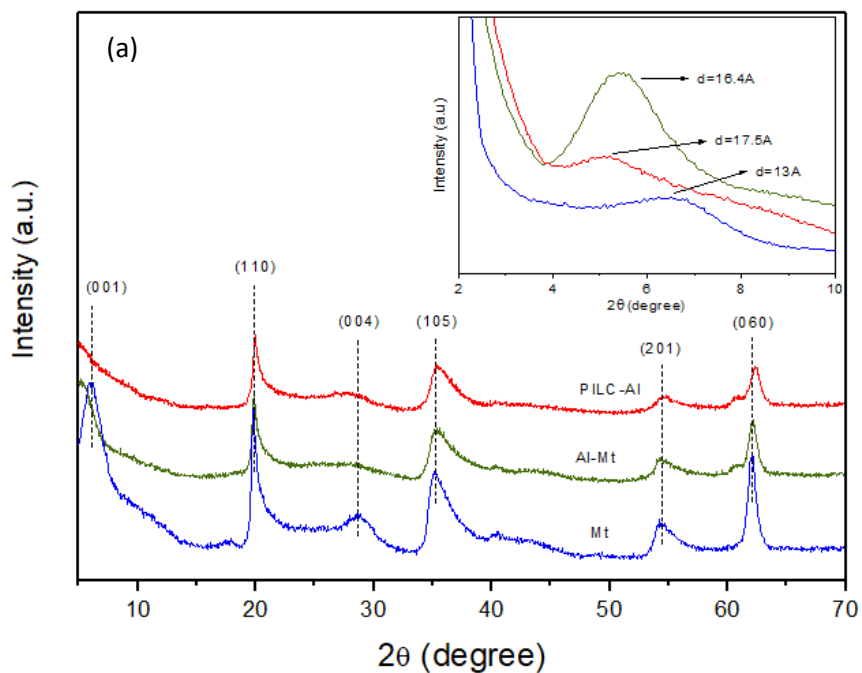
### 211 4.1 Structural and textural properties

212 X-ray diffraction patterns of the raw Mt and pillared-Mt samples are depicted in Figure 1a-b.  
213 Characteristic peaks of the pristine clay were observed as reported previously [30]. The  $d_{001}$  of  
214 the later is about 1.3 nm typical of one hydrated layer for Na-Mt. For PILC-A,  $d$  value  
215 increases from 1.3 nm to 1.64 nm suggesting an intercalation of the aluminium cations into  
216 the interlayer space of Mt. Upon calcination, the  $d_{001}$  value reached 1.75 nm due to the  
217 formation of oxide pillars as already reported [31,32].

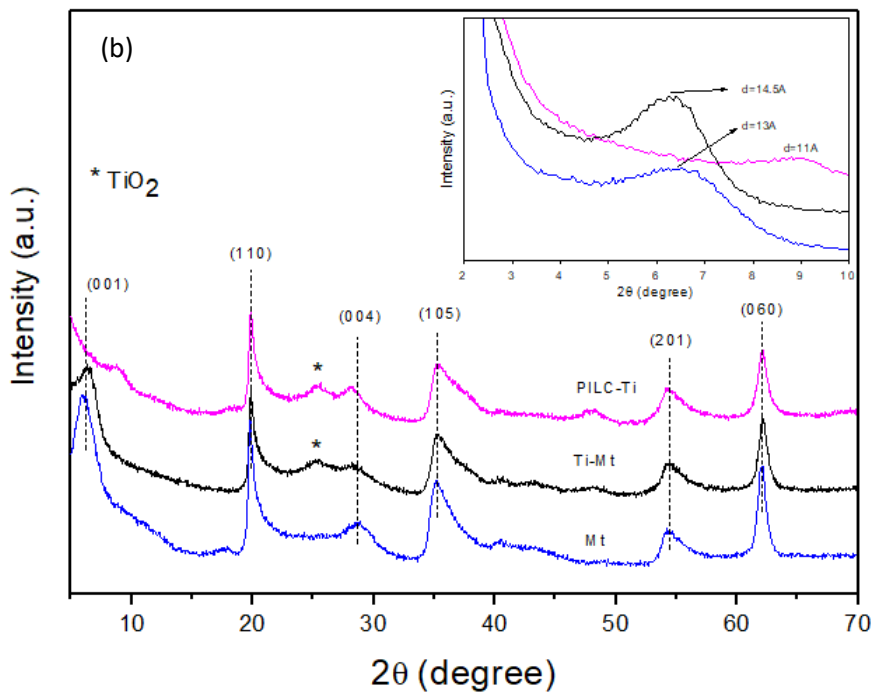
218 In the case of titanium cations, the  $d_{001}$  value varies from 1.3 nm to 1.45 nm (Figure 1b,  
219 insert) due to the increase of the interlayer space upon intercalation of titanium cations in Mt.  
220 After calcination, the (001) reflexion can not be observed anymore suggesting an  
221 heterogeneous stacking of the layer in the titanium pillared Mt samples [25,33] or an  
222 exfoliation. A peak at  $2\theta=25.36$  characteristic of anatase ( $\text{TiO}_2$ ) was observed as reported  
223 previously in Ti-pillared clay minerals [34–36].

224 After loading with dyes, no significant changes in the  $d_{001}$  values were found in the composite  
225 materials based on pillared-Mt and dyes.

226 It is known that modification of clays by pillarization with metal oxides also causes the  
227 increase of the specific area and promotes a permanent mesoporosity [37–39].



228



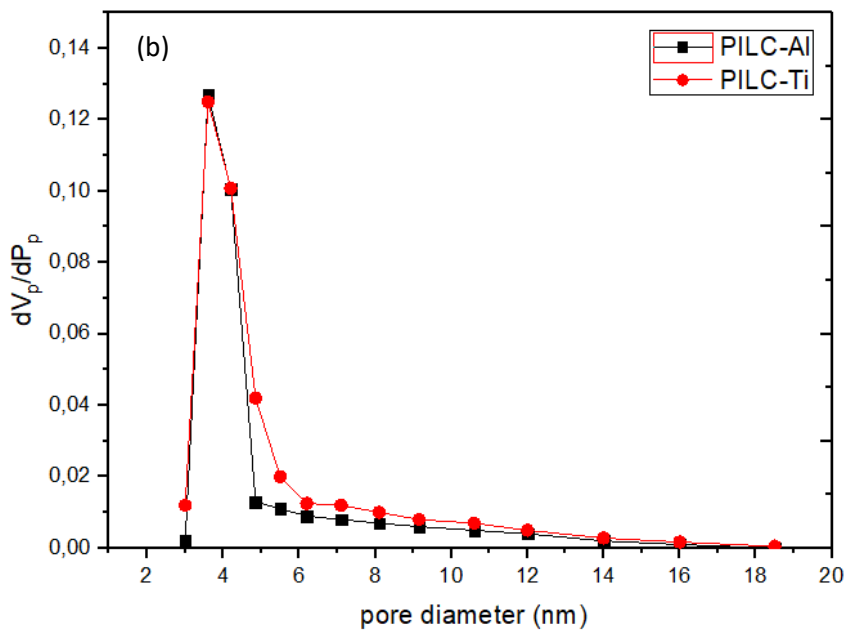
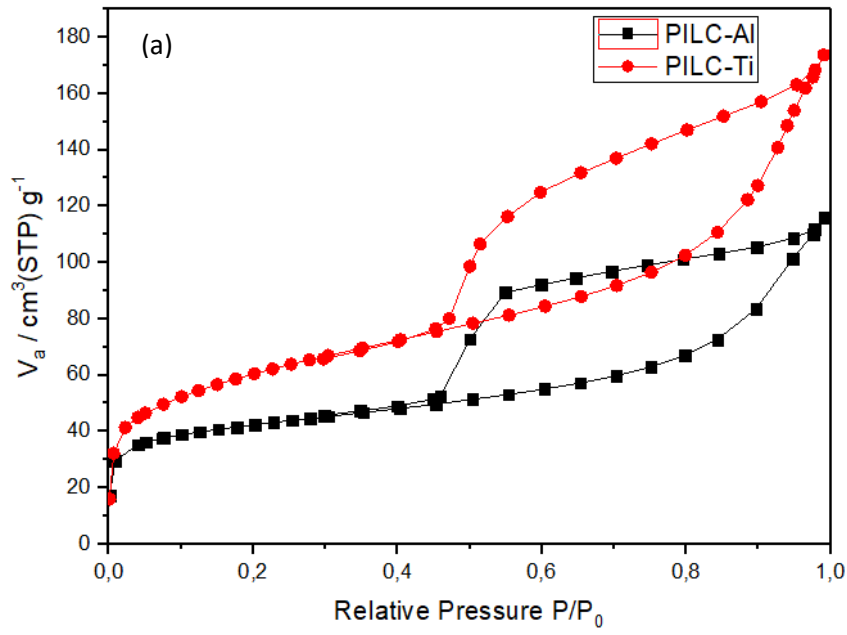
229

230 Figure 1. XRD patterns of pillared-Mt with (a) aluminium and (b) titanium cations, showing in insert  
231 the shift in the  $d_{001}$  peak upon metallic cations intercalation and upon calcination of the samples.

232

233 The N<sub>2</sub>-adsorption/desorption isotherms and pore size distribution of the pillared clays are  
234 presented in Figure 2a and 2b. The adsorption isotherms of the pillared samples fit the Type  
235 IV, for low relative pressures, the curve is characterized by a saturation step and presence of a  
236 hysteresis loop of type H<sub>4</sub> [34]. This kind of adsorption isotherm is typical of mesoporous  
237 materials [35]. The multipoint BET surface area (S<sub>BET</sub>) values were determined from isotherm  
238 data in the P/P<sub>0</sub> 0.09-0.5 range. The raw clay reached a surface area of 106 m<sup>2</sup>.g<sup>-1</sup>, while  
239 PILC-Al and PILC-Ti exhibited values of 186 m<sup>2</sup>.g<sup>-1</sup> and 204 m<sup>2</sup>.g<sup>-1</sup>, respectively. A narrow  
240 size distribution of the mesopores obtained by BJH method showed a diameter range between  
241 3-5 nm and 3-6 nm for the PILC-Al and PILC-Ti samples, respectively (Figure 2b). These  
242 results suggested that the pillaring process succeed in the PILC-Al and PILC-Ti samples.

243



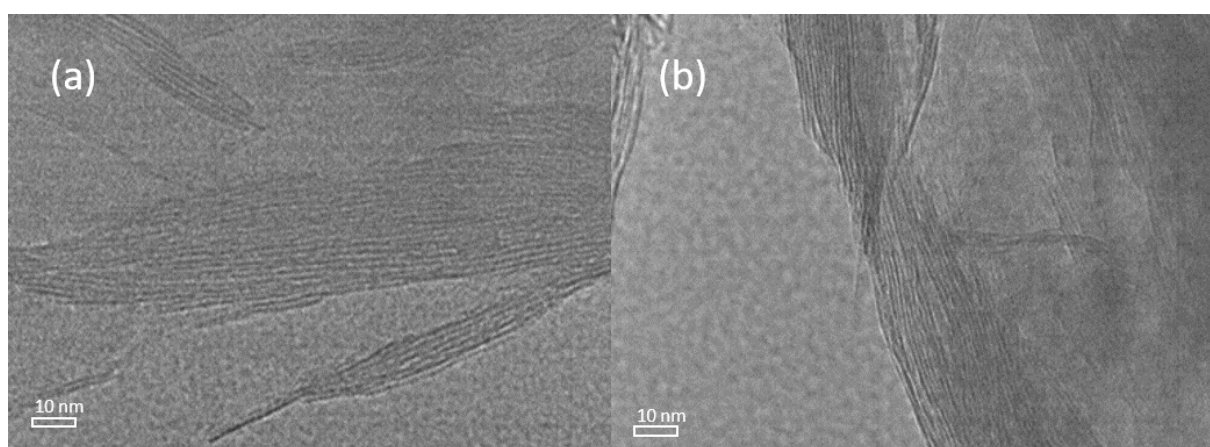
244

245 Figure 2. (a)  $\text{N}_2$  isotherms of adsorption/desorption at 77 K and (b) pore diameter ( $d_p$ ) distribution for  
 246 PILC-Al and PILC-Ti samples.

247

248 *4.2 Morphological analysis*

249 TEM experiments were performed to have a better view of the intercalation of the metal  
250 cations in the interlayer of montmorillonite. TEM images of Mt shows layered structures with  
251 alternate dark and bright fringes with a calculated interlayer distance of 1.26 nm for the raw  
252 sample. It was noticed that the distance increased to 1.75 nm and about 1.4-1.8 nm for PILC-  
253 Al and PILC-Ti samples, respectively (Figure 3a-b). The results suggested that the pillaring  
254 process occurs and that the lamellar structure of Mt was maintained for both samples, in  
255 agreement with the XRD results.

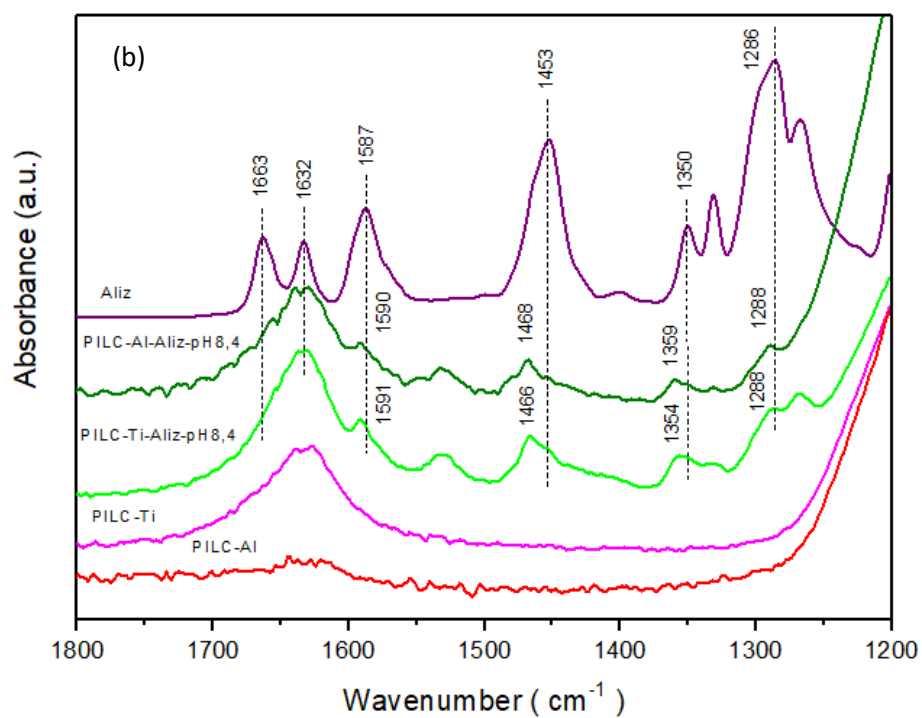
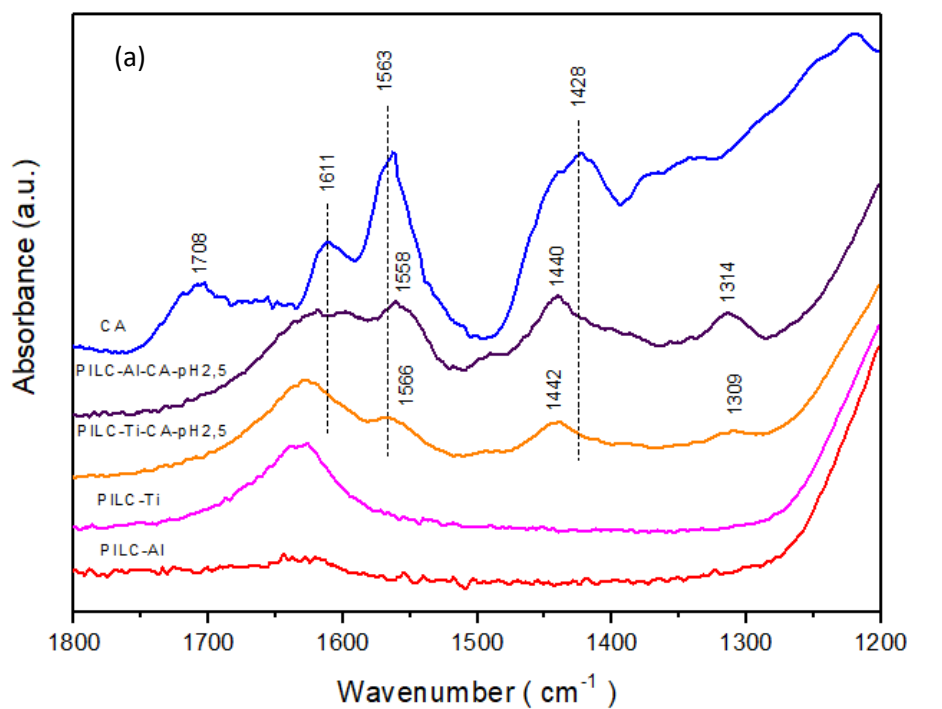


256  
257 Figure 3. TEM images of (a) PILC-Al and (b) PILC-Ti samples.

#### 258 4.3 ATR-Infrared

259 ATR-IR spectra of the pillared clay samples before and after adsorption of carminic acid and  
260 alizarin dyes are shown in Figure 4a-b. It can be noticed several characteristic bands of the  
261 dyes related to anthraquinone groups. Spectrum of bulk CA (Figure 4a) showed bands at 1611  
262  $\text{cm}^{-1}$ , 1563  $\text{cm}^{-1}$  and 1428  $\text{cm}^{-1}$  corresponding to the stretching vibration of  $\nu(\text{C}=\text{O})$  quinone  
263 group, stretching vibration of  $\nu(\text{C}=\text{C})$  aromatic and bending vibration of  $\delta(\text{OH})$  group,  
264 respectively. Bulk Aliz (Figure 4b) spectrum shows bands at 1663  $\text{cm}^{-1}$ , 1587  $\text{cm}^{-1}$  and 1453  
265  $\text{cm}^{-1}$  corresponding to the stretching vibration of  $\nu(\text{C}=\text{O})$  quinone group, stretching vibration  
266 of  $\nu(\text{C}=\text{C})$  aromatic and bending vibration to  $\delta(\text{OH})$  group, respectively [8]. Spectra of hybrid  
267 pigments with CA present shifts for some bands, in Figure 4a, the band of C=C structure

268 shifts from 1563 to 1558  $\text{cm}^{-1}$  in PILC-Al-CA-pH2.5 and to 1566  $\text{cm}^{-1}$  in PILC-Ti-CA-pH2.5.  
269 For the C=O function the band disappeared upon adsorption, the band corresponding to OH  
270 group is shifted from 1428 to 1440  $\text{cm}^{-1}$  in PILC-Al-CA-pH2.5 and to 1442  $\text{cm}^{-1}$  in PILC-Ti-  
271 CA-pH2.5. In the case of hybrid pigments with Aliz, in Figure 4b, the band assigned to the  
272 stretching vibration C=C aromatic shifts from 1587 to 1590  $\text{cm}^{-1}$  for PILC-Al-Aliz-pH8.4 and  
273 to 1591  $\text{cm}^{-1}$  in PILC-Ti-Aliz-pH8.4, the band corresponding to C=O group presented similar  
274 behaviour as CA, the band is not observed upon adsorption on clay. Finally, the band  
275 corresponding to bending vibration OH shift from 1453 to 1468  $\text{cm}^{-1}$  for PILC-Al-Aliz-pH8.4  
276 and to 1466  $\text{cm}^{-1}$  in PILC-Ti-Aliz-pH8.4. These results indicate that the coordinated bonds  
277 between anthraquinone groups and modified clay minerals can occur by chelation of  $\text{Al}^{3+}$  and  
278  $\text{Ti}^{4+}$  cations of the pillars with the quinone and catechol functions of the dyes as well as by  
279 adsorption of the dyes onto external and internal surface of clay mineral.



280

281 Figure 4. ATR-IR spectra of pillared clays and dyed clays with (a) carminic acid and (b) alizarin.

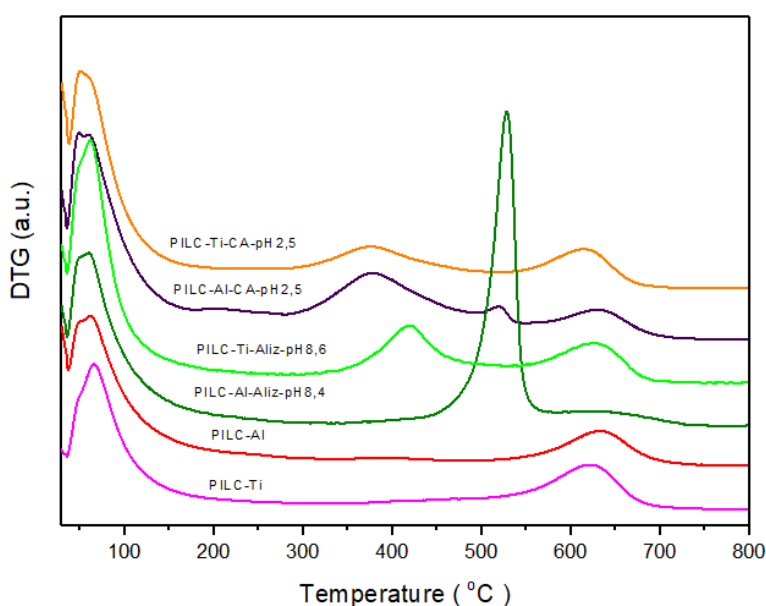
282

283 *Thermal Analyses*

284 DTG curves for all samples are depicted in Figure 5. The characteristic stages of the mass loss  
285 of water, organic matter and dehydroxylation, before and after adsorption of CA and Aliz  
286 dyes are shown.

287 Two regions of mass loss have been noticed for the raw Mt and pillared clays samples. The  
288 first one, with an endothermic event, with weight loss about 4.3-5 % at  $T_{max}=45$  °C is  
289 attributed to the departure of physisorbed water. The second at  $T_{max}=630$  °C, with an  
290 endothermic event, is attributed to structural dehydroxylation of the clay matrix with mass  
291 loss about 2.0 % for both samples [40].

292 After the dyeing process, the first peak corresponds to the dehydration with an amount  
293 between 6.5-8 %. The second peak between 350 and 560 °C for all samples corresponds to the  
294 oxidation of the organic matter. PILC-Ti dyed clays has 3.2 % of weight loss corresponding to  
295 alizarin dye and 3.5 % of carminic acid dye decomposition. PILC-Al dyed clays presents  
296 about 7.8 % of alizarin dye and 6.5 % of carminic acid dye decomposition. All the samples  
297 still show the peak related to dehydroxylation with a weight loss between 1.5-2.2 %.



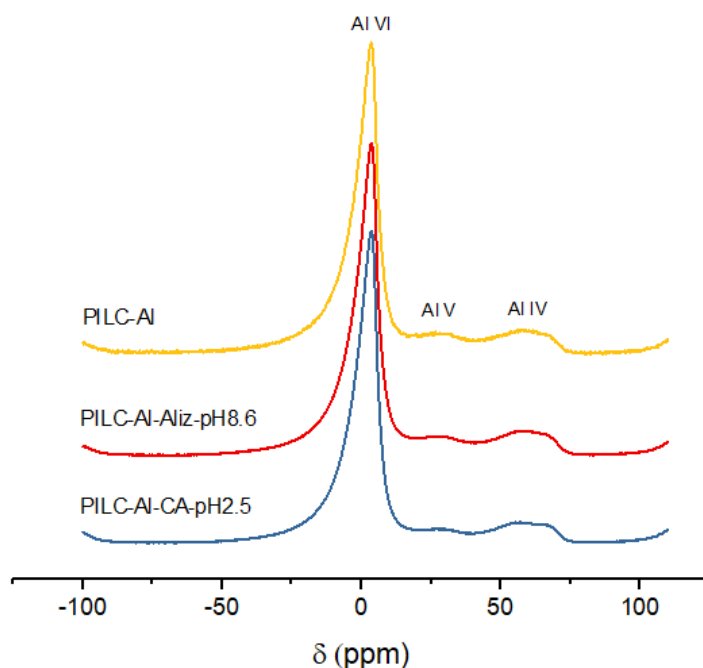
298

299 Figure 5. DTG curves for PILC-T, PILC-A, PILC-A-Aliz-pH8.6, PILC-T-Aliz-pH8.4, PILC-A-CA-pH2.5 and  
300 PILC-T-CA-pH2.5 dyed samples.

301

#### 302 4.5 Solid state nuclear magnetic resonance of $^{13}\text{C}$ and $^{27}\text{Al}$

303  $^{27}\text{Al}$  MAS NMR spectra of PILC-Al before and after adsorption of CA and Aliz dyes are  
304 depicted in Figure 6. PILC-Al sample presented three characteristic chemical shifts at 3.4  
305 ppm, 59.6 ppm and 28.6 ppm related to hexa-coordinated-Al (Al VI), tetra-coordinated-Al (Al  
306 IV) and penta-coordinated-Al (Al V), respectively. The intense peak of Al (VI) corresponds to  
307 the Al in the pillars and the Al (IV) signals are resulted of a overlap of the central Al in  $\text{Al}_{13}$   
308 (Keggin structure with a tetrahedral Al atom in the centre of the cluster coordinated to 4  
309 oxygen atoms) and small amount of Al in the tetrahedral sheets [24]. It has been noticed a  
310 shift from 3.4 to 3.3 ppm and from 3.4 to 3.2 ppm for PILC-Al-Aliz-pH8.4 and PILC-Al-CA-  
311 pH2.5 dyed samples, respectively. This may suggest the interactions between Aliz or CA and  
312 Si-OH-Al-OH in the Mt edges well as with pillars formation.

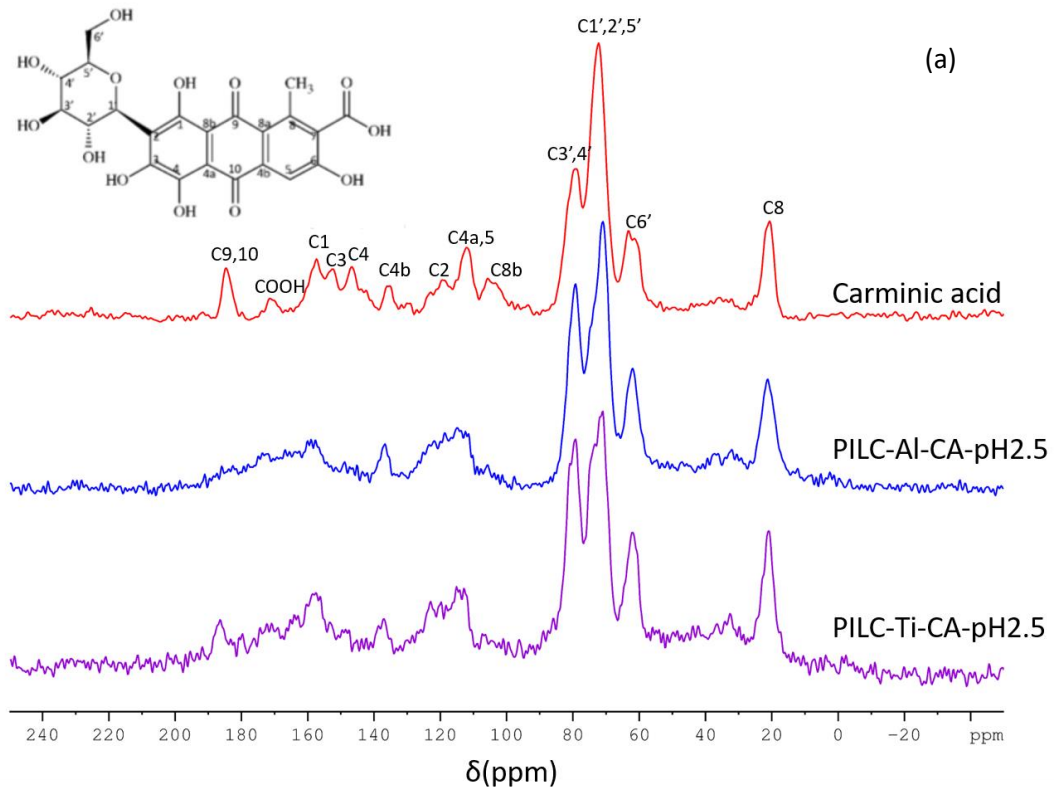


313

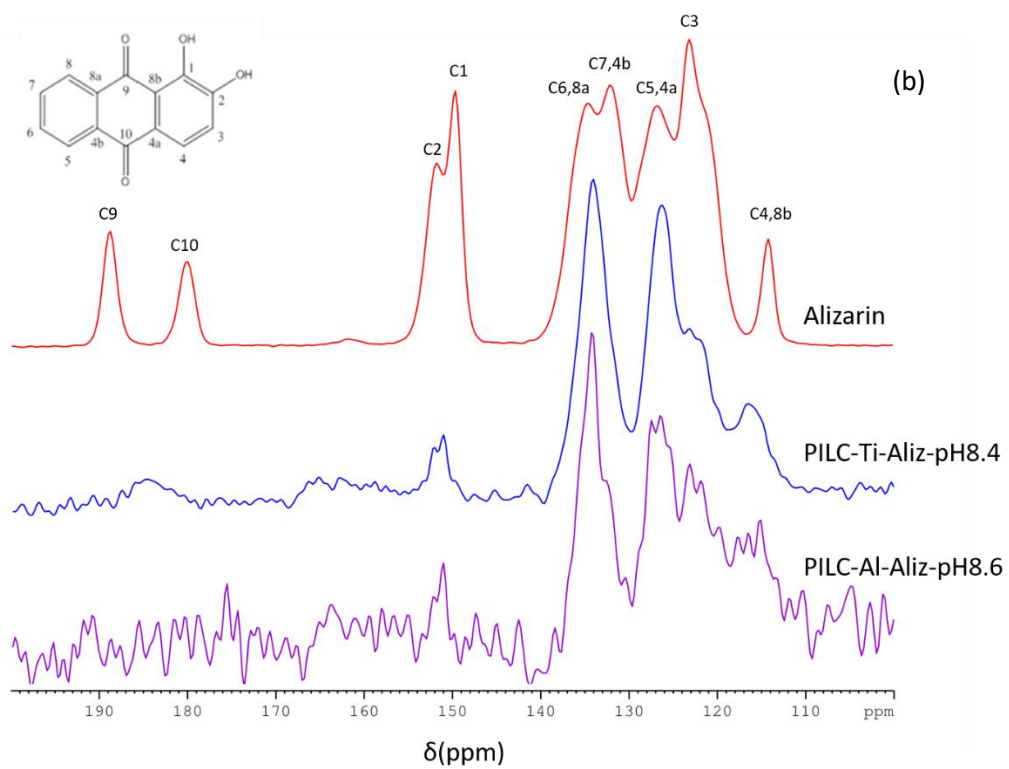
314 Figure 6.  $^{27}\text{Al}$  MAS NMR of PILC-Al before and after adsorption of CA and Aliz dyes.

315

316 <sup>13</sup>C MAS NMR spectra of the Al and Ti-pillared clay samples after adsorption with CA are  
317 presented in the Figure 7a. Although the spectra of the CA onto pillared clays composites  
318 exhibited almost the same signals than the raw dye, it was observed some changes in the  
319 chemical shifts. In bulk CA, the signal at 20.9 ppm is related to methyl group of C8 and the  
320 region between 60-80 ppm is attributed to the sugar part of the dye molecule. The signals at  
321 171.3 ppm and 185 ppm are assigned to the carboxylate moieties and to the ketones functions,  
322 respectively [1]. Some other shifts have been observed, upon complexation, such as from  
323 147.5 ppm to 149.2 ppm and 148.3 ppm, attributed to C4 signal for PILC-Al-CA-pH2.5  
324 sample and PILC-Ti-CA-pH2.5, respectively. The C5 signal is shifted from 112.5 to 115.2  
325 ppm and 114.1 ppm to PILC-Al-CA-pH2.5 and PILC-Ti-CA-pH2.5, respectively. In the  
326 region of the C9,10 the signal is not well defined for PILC-Al-CA-pH2.5 and is shifted from  
327 185 to 186.7 ppm for PILC-Ti-CA-pH2.5. This may suggest the chelation between the  
328 metallic cations and anthraquinone groups in the dyes. Indeed, dye may also be adsorbed in  
329 clay surface. The chromophore groups in anthraquinone dyes can also behave as binding  
330 functions between the dye molecule and the mineral support through an intermediate metal  
331 atom [9].



332



333

334 Figure 7. <sup>13</sup>C MAS NMR spectra of Al and Ti-pillared clays and dyed clays with (a) carminic acid and (b)  
 335 alizarin.

336

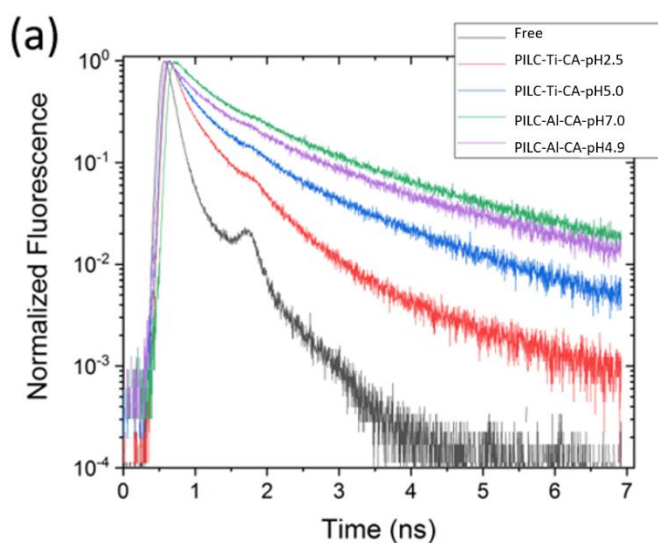
337  $^{13}\text{C}$  MAS NMR spectra of the Al and Ti-pillared clay samples after adsorption with Aliz are  
338 presented in the Figure 7b. Alizarin has distinct region for the resonances of the  
339 anthraquinone partial structure and hydroxy groups. The peaks corresponding to C1 and C2,  
340 that are assigned to hydroxyl groups, are shifted from 150 and 151.8 ppm to one signal at  
341 151.2 ppm and 151.4 ppm to PILC-Ti-Aliz-pH8.4 and PILC-Al-Aliz-pH8.6, respectively. It  
342 was notice that the signals assigned to C9 and C10 corresponding to ketone functions shifts to  
343 shoulder not well defined at approximately 184 ppm in both pillared clays. The results  
344 suggested that the ketone and hydroxyl groups of the dyes can be main attachment site with  
345 the modified inorganic matrix [41,42].

#### 346 *4.6 Fluorescence analysis*

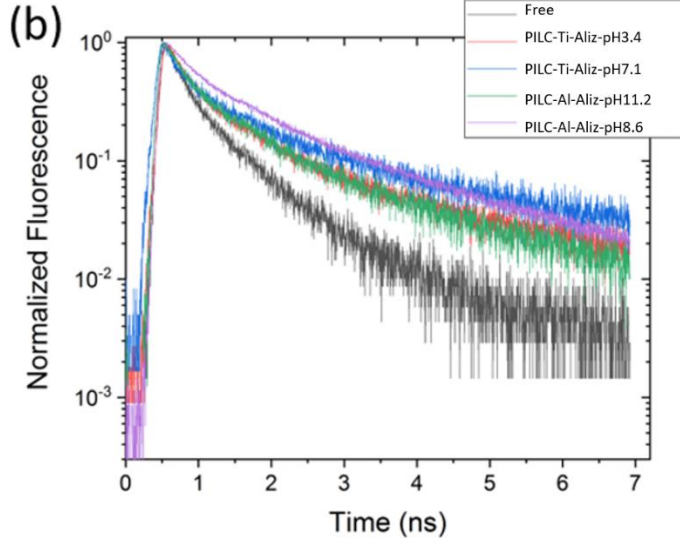
347 The time resolved fluorescence characterisation of carminic acid and alizarin free in solution  
348 and loaded on pillared clay were performed under wavelength excitation 540 nm and 550 nm  
349 respectively (Figure 8). Free in solution, the average fluorescence lifetimes are 0.151 ns and  
350 0.596 ns for carminic acid and alizarin, respectively. They significantly increase after  
351 adsorption on pillared clay (tables I and II). This result confirms a stabilisation of both dyes  
352 due to their interactions with the clay as shown by NMR.

353 The fluorescence decay of the alizarin free in solution and adsorbed on all materials requires  
354 three components to be fitted. For the PILC-Ti, similar results were obtained at pH 7.1 and  
355 3.4 suggesting similar interactions between the dye and the pillared clay. On the contrary, for  
356 PILC-Al the pH influences the fluorescence lifetime and thus the interaction are not the same,  
357 due different degrees of protonation of the molecule in these pH. The different lifetimes at pH  
358 around 7-8 for PILC-Ti and PILC-Al dyed with Alizarin confirms that the cation (Al or Ti) is  
359 involved in the interaction material/dyes.

360 For the carminic acid, the fluorescence results are quite different. In solution, the fluorescence  
361 decay is composed by three lifetimes (0.496 ns, 0.099 ns, and 0.048 ns). After loading on  
362 pillared clays, it requires four components among them one component longer than 1.5 ns  
363 appears. It also depends on the metal cations used for the pillaring process confirming its role  
364 in the material/dye interaction. Moreover, the degree of protonation influences the  
365 fluorescence emission properties. Indeed, for PILC-Ti-pH5 the average lifetime is 0.945 ns  
366 and the longer component represents 25.6 % of the global decay while for PILC-Ti-pH2.5 the  
367 average lifetime is shorter (0.469 ns) and the longer component 1.723 ns represents less than  
368 10 %. At pH 5, the carboxyl group is deprotonated and thus can be coordinated with  
369 aluminium by electrostatic interactions. On the contrary at pH 2.5 the carminic acid is totally  
370 protonated and thus the complexation with aluminium likely involved the anthraquinone  
371 and/or clay surface as suggested by NMR study.



372



373

374 Figure 8: Fluorescence decays of carminic acid (a) and alizarin (b) free in solution and  
 375 loaded on different pillared clays.

376

377

378 Table I: Fluorescent lifetime ( $\tau_i$ ) and average lifetime ( $\tau_{AV}$ ) results for carminic acid free in solution and  
 379 loaded on pillared clay for excitation wavelength 540 nm at emission wavelength 600nm ( $\lambda_e$ ) Yield =  
 380  $100\alpha_i\tau_i/\sum\alpha_i\tau_i$  represents the contribution of each emission to the total emission

Samples	$\tau_1$ (ns) / (yield)	$\tau_2$ (ns) / (yield)	$\tau_3$ (ns) / (yield)	$\tau_4$ (ns) / (yield)	$\tau_{(av)}$ (ns)	$\chi^2$
CA-H <sub>2</sub> O	0.496 (15.9%)	0.099 (62.7%)	0.048 (21.4)	-	0.151	0.87
PILC-Ti-CA-pH5	2.202 (25.6%)	0.774 (40%)	0.270 (24.6%)	0.059 (9.9%)	0.945	1.08
PILC-Ti-CA-pH2.5	1.723 (9.6%)	0.496 (53.2%)	0.147 (22.2%)	0.047 (15%)	0.469	1.00
PILC-Al-CA-pH4.9	2.798 (33.7%)	0.981 (41.8%)	0.326 (20.5%)	0.053 (4.1%)	1.421	1.02
PILC-Al-CA-pH7	2.91 (37.3%)	1.014 (43.9%)	0.322 (16.1%)	0.048 (2.6%)	1.584	0.99

381

382 Table II: Fluorescent lifetime ( $\tau_i$ ) and average lifetime ( $\tau_{AV}$ ) results for alizarin free in solution and  
 383 loaded on pillared clay for excitation wavelength 540 nm at emission wavelength 600nm ( $\lambda_e$ ) Yield =  
 384  $100\alpha_i\tau_i/\sum\alpha_i\tau_i$  represents the contribution of each emission to the total emission

Samples	$\tau_1$ (ns) / (yield)	$\tau_2$ (ns) / (yield)	$\tau_3$ (ns) / (yield)	$\tau_{(av)}$ (ns)	$\chi^2$
Aliz-H <sub>2</sub> O	1.094 (37.7%)	0.359 (49.1%)	0.059 (13.2%)	0.596	0.84

PILC-Al-Aliz-pH11.2	2.315 (45.3%)	0.585 (42.5%)	0.125 (12.2%)	1.313	1.09
PILC-Al-Aliz-pH8.4	2.78 (48.5%)	0.846 (41.7%)	0.189 (9.8%)	1.721	1.00
PILC-Ti-Aliz-pH3.4	3.217 (42.2%)	0.713 (39.5%)	0.183 (18.2%)	1.674	1.26
PILC-Ti-Aliz-pH7.1	3.372 (54.5%)	0.749 (32.6%)	0.183 (12.9%)	2.105	1.30

385

#### 386 4.7 Colours and hue of pigments

387 The colours and hue variation of the pillared samples upon CA and Aliz adsorption were pH  
388 dependent (Figure 9). It is known that carminic acid presents three different values of pK<sub>a</sub>  
389 (2.8, 5.4 and 8.1) and alizarin has two different values (6.6-7.5 and 12.4-13.5). In solution,  
390 Aliz occurs in the form of partially dissociated yellow molecules at pH below 5.2. At pH 6-10  
391 it is deprotonated and occurs in red monovalent cations. Finally, it occurs in the violet di-  
392 anionic form at pH about 12 [43]. In turn, CA is present, in acid pH, in the orange  
393 monoanionic form. Indeed, CA bears one negative charge at pH about 4 and is entirely  
394 negative in neutral medium [1]. At pH 8, it is completely deprotonated and is present, in  
395 solution, in the violet colour tri-anionic molecule. From these observations, at low values of  
396 pH the interactions between organic dyes and clay surface is globally driven by electrostatic  
397 forces. Whereas at higher values of pH the interactions can occur through complexation of the  
398 catechol and hydroxy-keto groups of chromophore structures with the metallic cations of the  
399 pillars present in the interlamellar spaces of montmorillonite. Furthermore, it is also known  
400 that intensity of colours is dependent of the amount of the adsorbed organic dye.



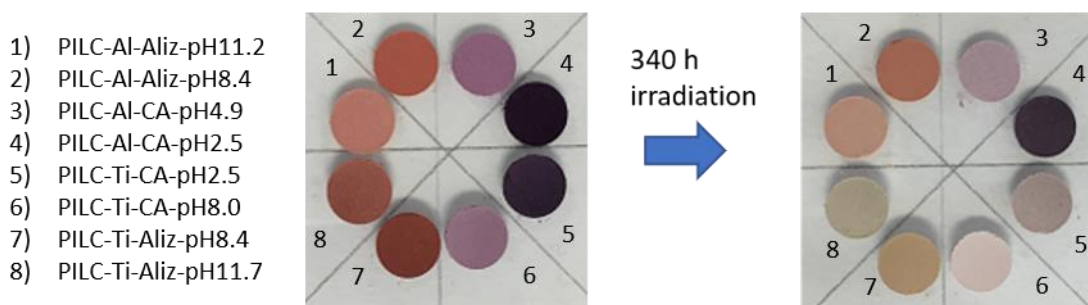
401

402 Figure 9. Colours of pigments obtained at different pH for organic dyes onto modified clay (a) PILC-A-  
 403 Aliz-pH11.2; (b) PILC-A-CA-pH2.5; (c) PILC-T-Aliz-pH8.4 and (d) PILC-T-CA-pH8.0.

404

405 *4.8 Light-Induced Aging*

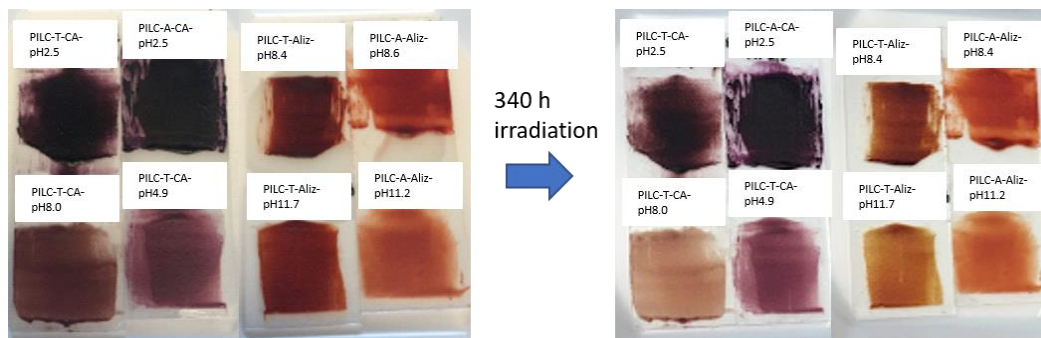
406 Light can be essential for appreciation of artworks, but in long time it may induces  
 407 deterioration to paintings or other artefacts, causing irreversible damage which may include  
 408 colour fading. Light exposure causes photooxidative degradation resulting in the breakdown  
 409 of the dye molecules [44]. Then, the colours of solid pigments and oil painting prepared were  
 410 evaluated before and after light exposure during 340 hours, where this time is equivalent to  
 411 approximately 28 years of exposure in a museum (Figure 10a-b).



412

413 Figure 10(a). Solid pigments samples before and after LED irradiation based Aliz and CA dyes  
 414 adsorbed onto Al-pillared clay (top) and Ti-pillared clay (bottom).

415



416

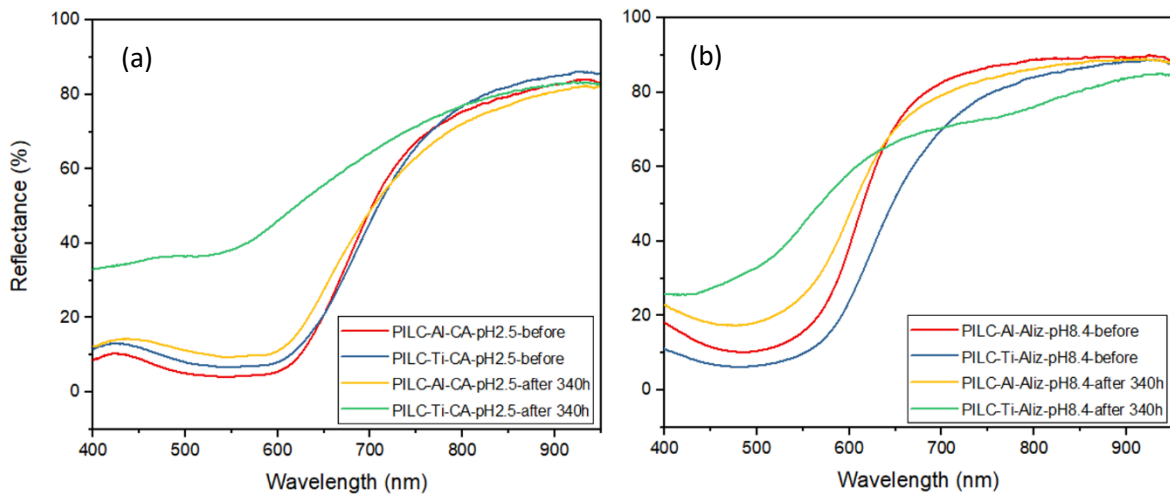
417 Figure 10(b). Oil paint formulations unexposed and exposed LED irradiation. Hybrid pigments based  
 418 Aliz and CA organic dyes onto pillared clays.

419

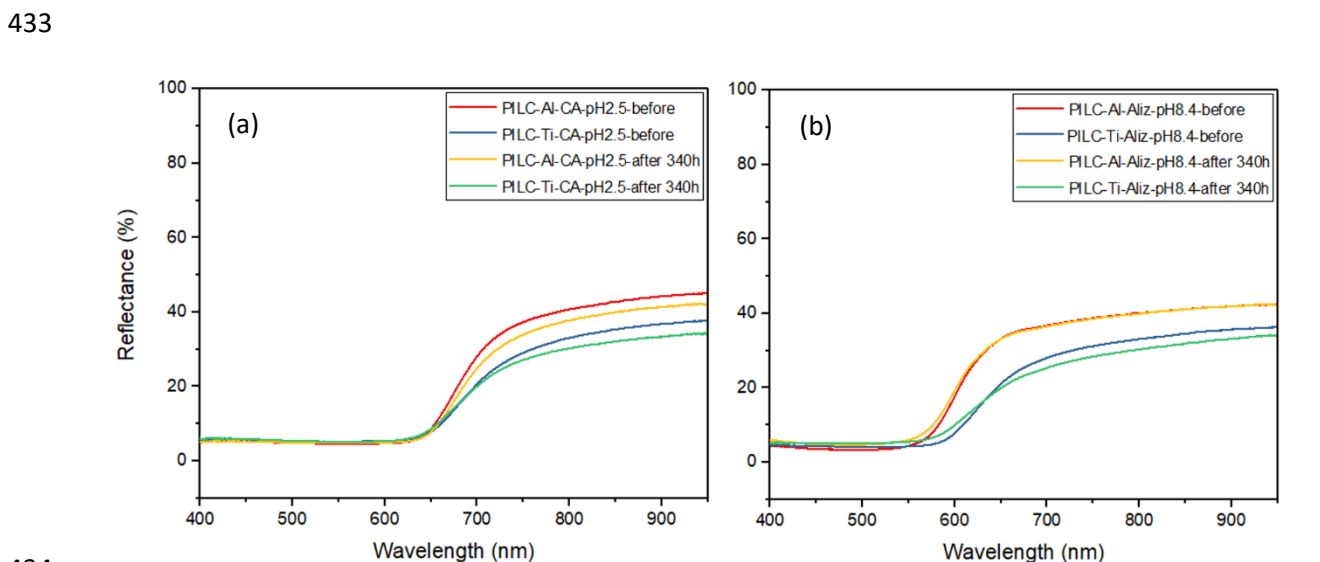
420 The spectral reflectance distribution curve of hybrid pigments, before and after photoaging  
 421 test, are shown in Figure 11 and 12. In general, all samples present similar spectra. The  
 422 differences are observed for PILC-Ti-CA-pH2.5 and PILC-Ti-Aliz-pH8.4 solid pigment  
 423 where after light exposure, a shift at higher values of reflectance is observed. It is probably  
 424 due to the degradation/fading of the dye as observed in Figure 11. Oil painting samples had  
 425 lower reflectance values compared to the solid pigments and all samples present very similar  
 426 reflectance spectrum, according to Figure 12, suggesting less variation of colors consequently  
 427 high resistance of the formulations even after a long time of irradiation.

428

429



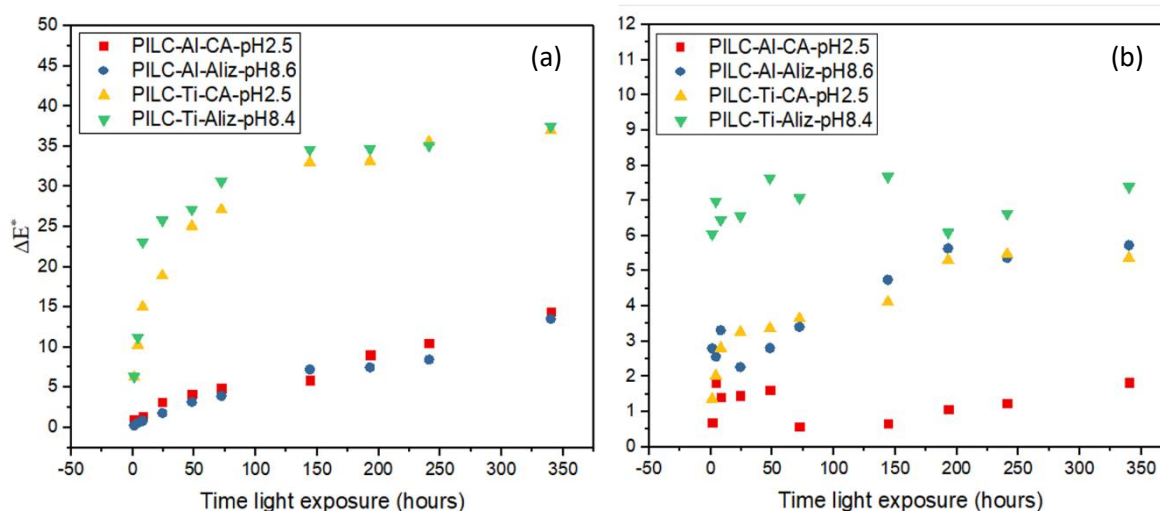
430  
 431 Figure 11. Reflectance spectrum of solid pigments before and after light exposure for 340 h for (a)  
 432 carminic acid and (b) alizarin dyed samples.



434  
 435 Figure 12. Reflectance spectra of oil paintings formulation before and after light exposure for 340 h  
 436 for (a) CA and (b) Aliz dyed samples.

437  
 438 The measurement over CIE  $L^*$ ,  $a^*$  and  $b^*$  scales notices a quantitative change over the  
 439 pigments.  $\Delta E^*$  variation values are due to the change of pigment structure after light exposure.  
 440 Higher values of  $\Delta E^*$  are observed for solid pigments (Figure 13a). Indeed,  $\Delta E^* < 14$  for dyes  
 441 adsorbed on PILC-Al samples and  $\Delta E^* < 36$  for dyes adsorbed in PILC-Ti clays are noticed.  
 442 Al-pillared based pigments have been shown more stable than Ti-pillared based. This may  
 443 probably due to the photocatalytic property of the anatase phase that remains even after the

444 complexation of the pillared material with the dye molecule. In all samples, lower values of  
 445  $\Delta E^*$  are observed for oil paint formulations, mainly aluminium based samples (Figure 13b).  
 446 These results suggested high stability of the ink formulations upon incorporation of drying oil,  
 447 probably the linseed oil in the surface of the pigment, disturbs the reactions with oxygen.  
 448 When irradiation is performed in air, the clay will have much faster access to new oxygen  
 449 coming from outside which would result in higher dye photobleaching rates at that region [45]  
 450 because the oxygen seems to play a key role for the dye photostability. Linseed oil can be  
 451 acting as an inhibitor in the formation of the radicals, forming a photoresist protective layer.



452  
 453 Figure 13. Colour difference ( $\Delta E^*$ ) between (a) solid pigments and (b) oil painting formulation  
 454 samples exposed to the light-induced aging for 340 h.

455  
 456 According to these results, after light exposure, fading occurs in the solid pigments, especially  
 457 in samples pillarized with titanium cations. Aluminum-based samples are more stable due to  
 458 the strong interactions between the dye molecules and the modified clay, that retard  
 459 photodegradation. The painting formulations exhibit minor variations in the  $L^*$ ,  $a^*$  and  $b^*$   
 460 parameters after a long period of exposure to light, perhaps the formulations inhibit the  
 461 hydroperoxides formation that accelerate the photo-oxidation process [46].

462

## 463 **5.0 CONCLUSIONS**

464

465 Hybrid pigments were prepared by stabilization of organic dyes onto pillared  
466 montmorillonite. XDR, TEM and BET analyses suggest that pillaring process occurs. The  
467 interactions between chromophore groups and clay surface is driven by electrostatic forces  
468 and/or complexation between metallic cations in the interlamellar space and ketone and  
469 hydroxyl functions in the dye molecule. These results were highlighted by Infrared and NMR  
470 experiments. Fluorescence analysis report that increase of average lifetime for dyes upon  
471 adsorption on modified clay confirm interactions between organic dyes and clay mineral and  
472 underline the strong dependence on the speciation. Different parameters influence the color  
473 and hue of the hybrids the pH, the amount of the adsorbed dyes and the nature of metallic  
474 cations in the interlayer space. Oil paint formulations simulate real materials used in  
475 paintings. High stability of the organic-inorganic hybrids, especially from aluminium pillared  
476 clays dyed with carminic acid and alizarin, indicate that these can be applied as new stable  
477 lake pigments.

478

## 479 **6.0 ACKNOWLEDGEMENTS**

480 We acknowledge the financial support from the CAPES/COFEBUB (Project n° 835/15). The  
481 authors thank the Île-de-France region and CNRS for funding.

482

## 483 **7.0 REFERENCES**

484

485 [1] Fournier F, de Viguerie L, Balme S, Janot JM, Walter P, Jaber M. Physico-chemical

- 486 characterization of lake pigments based on montmorillonite and carminic acid. *Applied*  
487 *Clay Science* 2015;130:12–7.
- 488 [2] Bechtold T and Mussak R. *Handbook of Natural Colorants* 2009, Wiley, United  
489 Kingdom.
- 490 [3] Tian G, Wang W, Wang D, Wang Q, Wang A. Novel environment friendly inorganic  
491 red pigments based on attapulgite. *Powder Technology* 2017;315:60–7.
- 492 [4] Cao L, Fei X, Zhao H. Dyes and Pigments Environmental substitution for PbCrO<sub>4</sub>  
493 pigment with inorganic-organic hybrid pigment. *Dyes and Pigments* 2017;142:100–7.
- 494 [5] Pereira F, Sousa K, Cavalcanti G, França D, Queiroga L, Santos I, Fonseca M, Jaber  
495 M. Green biosorbents based on chitosan-montmorillonite beads for anionic dye  
496 removal. *Journal of Environmental Chemical Engineering* 2017;5:3309–18.
- 497 [6] Thangaraj V, Bussiere J, Janot JM, Bechelany M, Jaber M, Subramanian S, et al.  
498 Fluorescence Quenching of Sulforhodamine Dye over Graphene Oxide and Boron  
499 Nitride Nanosheets. *European of Journal Inorganic Chemistry* 2016;2016:2125–30.
- 500 [7] Zhang A, Mu B, Luo Z, Wang A. Dyes and Pigments Bright blue halloysite / CoAl<sub>2</sub>O<sub>4</sub>  
501 hybrid pigments : Preparation , characterization and application in water-based  
502 painting. *Dyes and Pigments* 2017;139:473–81.
- 503 [8] Pérez E, Ibarra IA, Guzmán A, Lima E. Hybrid pigments resulting from several guest  
504 dyes onto  $\gamma$ -alumina host: A spectroscopic analysis. *Spectrochimica Acta Part A Mol*  
505 *ecular and Biomolecular Spectroscopy* 2017;172:174–81.
- 506 [9] Claro A, Melo MJ, Schäfer S, de Melo JSS, Pina F, van den Berg KJ, et al. The use of  
507 microspectrofluorimetry for the characterization of lake pigments. *Talanta*

- 508 2008;74:922–9.
- 509 [10] Perez-Ramirez E, Lima E, Guzman A. Natural betalains supported on  $\gamma$ -alumina: A  
510 wide family of stable pigments. *Dyes and Pigments* 2015;120:161–8.
- 511 [11] Anselmi C, Capitani D, Tintaru A, Doherty B, Sgamellotti A, Miliani C. Beyond the  
512 color : A structural insight to eosin-based lakes. *Dyes and Pigments* 2017;140:297–311.
- 513 [12] Mintova S, Jaber M, Valtchev V. Nanosized microporous crystals: emerging  
514 applications. *Chemical Society Reviews* 2015;44:7207–33.
- 515 [13] El Adraa K, Georgelin T, Lambert JF, Jaber F, Tielens F, Jaber M. Cysteine-  
516 montmorillonite composites for heavy metal cation complexation: A combined  
517 experimental and theoretical study. *Chemical Engineering Journal* 2017;314:406–17.
- 518 [14] Arnold, D.E. Maya Blue and Palygorskite: A second possible pre-Columbian source.  
519 *Ancient Mesoamerica* 2005, 16, 51–62.
- 520 [15] Coccoletzi GH, Canto G. Trapping and diffusion of organic dyes inside of palygorskite  
521 clay: The ancient Maya Blue pigment. *Microporous and Mesoporous Materials*  
522 2017;249.
- 523 [16] Wu S, Duan Z, Hao F, Xiong S, Xiong W, Lv Y, et al. Preparation of acid-activated  
524 sepiolite / Rhodamine B @ SiO<sub>2</sub> hybrid fluorescent pigments with high stability.  
525 *Dyes and Pigments* 2017;137:395–402.
- 526 [17] Tian, G., Wang, W., Mu, B., Wang, Q., Wang, A., 2017a. Cost-efficient, vivid and stable  
527 red hybrid pigments derived from naturally available sepiolite and halloysite. *Ceramics*  
528 *International* 43, 1862–1869.
- 529 [18] Kittinaovarat S, Kansomwan P, Jiratumnukul N. Chitosan / modified montmorillonite

- 530 beads and adsorption Reactive Red 120. *Applied Clay Science* 2010;48:87–91.
- 531 [19] Jaber, M., Georgelin, T., Bazzi, H., Costa-torro, F., Clodic, G., 2014. Selectivities in  
532 adsorption and peptidic condensation in the (arginine and glutamic acid)/montmorillonite  
533 clay system. *Journal of Physical Chemistry C* 118, 44, 25447-25455
- 534 [20] Gil A, Assis FCC, Albeniz S, Korili SA. Removal of dyes from wastewaters by  
535 adsorption on pillared clays. *Chemical Engineering Journal* 2011;168:1032–40.
- 536 [21] Gil A, Gandía LM, Vicente MA. Recent Advances in the Synthesis and Catalytic  
537 Applications of Pillared Clays. *Catalysis Reviews*, 2017;4940.
- 538 [22] Li K, Lei J, Yuan G, Weerachanchai P, Wang JY, Zhao J, et al. Fe-, Ti-, Zr- and Al-  
539 pillared clays for efficient catalytic pyrolysis of mixed plastics. *Chemical Engineering*  
540 *Journal* 2017;317:800–9.
- 541 [23] Tangaraj V, Janot J, Jaber M, Bechelany M, Balme S. Adsorption and photophysical  
542 properties of fluorescent dyes over montmorillonite and saponite modified by  
543 surfactant. *Chemosphere* 2017, 184 1355-1361.
- 544 [24] Bergaoui L, Lambert J-F, Suquet H, Che M. CuII on Al13-Pillared Saponites:  
545 Macroscopic Adsorption Measurements and EPR Spectra. *Journal of Physical*  
546 *Chemistry*. 1995;99:2155–61.
- 547 [25] Tomul F, Turgut Basoglu F, Canbay H. Determination of adsorptive and catalytic  
548 properties of copper, silver and iron contain titanium-pillared bentonite for the removal  
549 bisphenol A from aqueous solution. *Applied Surface Science* 2016;360:579–93.
- 550 [26] MacHatova, Z., Barbierikova, Z., Poliak, P., Jancovicova, V., Lukes, V., Brezova, V.,  
551 2016. Study of natural anthraquinone colorants by EPR and UV/vis spectroscopy. *Dyes*

552 and Pigments 132, 79–93

553 [27] Miliani, C., Romani, a, Favaro, G., 2000. Acidichromic effects in 1, 2-di-and 1, 2, 4-  
554 trihydroxyanthraquinones. A spectrophotometric and fluorimetric study. Journal of  
555 Physical Organic Chemistry 141–150.

556 [28] Vágvölgyi V, Kovács J, Horváth E, Kristóf J, Makó É. Investigation of  
557 mechanochemically modified kaolinite surfaces by thermoanalytical and spectroscopic  
558 methods. Journal of Colloids and Interface Science 2008;317:523–9.

559 [29] Balme S, Guégan R, Janot J-M, Jaber M, Lepoitevin M, Dejardin P, et al. Structure,  
560 orientation and stability of lysozyme confined in layered materials. Soft Matter  
561 2013;9:3188.

562 [30] Cornu, D., Lin, L., Daou, M.M., Jaber, M., Krafft, J.-M., Herledan, V., Laugel, G.,  
563 Millot, Y., Lauron-Pernot, H., 2017. Influence of acid–base properties of Mg-based  
564 catalysts on transesterification: role of magnesium silicate hydrate formation. Catalysis  
565 Science Technology 7, 1701–1712.

566 [31] Ksontini N, Ñ WN, Ghorbel A. Al – Fe pillared clays : Synthesis , characterization and  
567 catalytic wet air oxidation activity. Journal of Physics and Chemistry of Solids  
568 2008;69:1112–5.

569 [32] Kumararaja P, Manjaiah KM, Datta SC, Sarkar B. Remediation of metal contaminated  
570 soil by aluminium pillared bentonite : Synthesis , characterisation , equilibrium study  
571 and plant growth experiment. Applied Clay Science 2017;137:115–22.

572 [33] Ooka C, Akita S, Ohashi Y, Horiuchi T, Suzuki K, Komai S, et al. Crystallization of  
573 hydrothermally treated TiO<sub>2</sub> pillars in pillared montmorillonite for improvement of the  
574 photocatalytic activity. Journal of Materials Chemistry 1999:2943–52.

- 575 [34] Barama S, Davidson A, Barama A, Boukhrouf H, Casale S, Calers C, et al.  
576 Dephosphatation under UV light of water by Ti-PILC with activation by secondary  
577 species (La, Se, and Rb). *Comptes Rendus Chimie* 2017;20:7–19.
- 578 [35] Liang X, Qi F, Liu P, Wei G, Su X, Ma L, et al. Performance of Ti-pillared  
579 montmorillonite supported Fe catalysts for toluene oxidation: The effect of Fe on  
580 catalytic activity. *Applied Clay Science*, 2016;132–133:96–104.
- 581 [36] Chmielarz L, Piwowarska Z, Kuśtrowski P, Wegrzyn A, Gil B, Kowalczyk A, et al.  
582 Comparison study of titania pillared interlayered clays and porous clay heterostructures  
583 modified with copper and iron as catalysts of the DeNOx process. *Applied Clay*  
584 *Science*, 2011;53:164–73.
- 585 [37] Bergaoui L, Lambert JF, Vicente-Rodriguez MA, Michot LJ, Villiéras F. Porosity of  
586 Synthetic Saponites with Variable Layer Charge Pillared by Al-13 Polycations.  
587 *Langmuir*, 1995;11:2840–52.
- 588 [38] Hutson ND, Hoekstra MJ, Yang RT. Control of microporosity of Al O<sub>3</sub>-pillared clays :  
589 effect of pH , calcination temperature and clay cation exchange capacity. *Microporous*  
590 *and Mesoporous Materials*, 80, 1999;28:447–59.
- 591 [39] Roca Jalil ME, Baschini M, Rodríguez-Castellón E, Infantes-Molina A, Sapag K.  
592 Effect of the Al/clay ratio on the thiabendazol removal by aluminum pillared clays.  
593 *Applied Clay Science* 2014;87:245–53.
- 594 [40] Giustetto R, Wahyudi O, Corazzari I, Turci F. *Applied Clay Science* Chemical stability  
595 and dehydration behavior of a sepiolite / indigo Maya Blue pigment. *Applied Clay*  
596 *Science*, 2011;52:41–50.
- 597 [41] Doscocz M, Kubas K, Frackowiak A, Gancarz R. NMR and ab initio studies of Mg<sup>2+</sup>,

- 598 Ca<sup>2+</sup>, Zn<sup>2+</sup>, Cu<sup>2+</sup> alizarin complexes. *Polyhedron* 2009;28:2201–5.
- 599 [42] Fain, V.Y., Zaitsev, B.E., Ryabov, M. a, 2004. Metal Complexes with 1, 5- and  
600 Electronic Absorption Spectra and Structure of Ligands, *Russian Journal of Coordination*  
601 *Chemistry* 30, 385–389.
- 602 [43] Epstein M, Yariv S. Visible-spectroscopy study of the adsorption of alizarinate by Al-  
603 montmorillonite in aqueous suspensions and in solid state. *Journal of Colloids Interface*  
604 *Science*, 2003;263:377–85.
- 605 [44] Feng W, Nansheng D, Helin H. Degradation mechanism of azo dye C. I. reactive red 2  
606 by iron powder reduction and photooxidation in aqueous solutions. *Chemosphere*  
607 2000;41:1233–8.
- 608 [45] Lencione D, Gehlen MH, Trujillo LN, Leitao RCF, Albuquerque RQ. The spatial  
609 distribution of the photostability of thionine in zeolite L nanochannels investigated by  
610 Photobleaching Lifetime Imaging Microscopy. *Photochemical and Photobiology*  
611 *Science*, 2016;15:398–404.
- 612 [46] Wu T, Liu G, Zhao J, Hidaka H, Serpone N. Evidence for H<sub>2</sub>O<sub>2</sub> Generation during the  
613 TiO<sub>2</sub>-Assisted Photodegradation of Dyes in Aqueous Dispersions under Visible Light  
614 Illumination. *Journal of Physical Chemistry B* 1999;103:4862–7.